


Article

Graphene Oxide Composite for Selective Recognition, Capturing, Photothermal Killing of Bacteria over Mammalian Cells

Gang Ma ¹, Junjie Qi ^{1,*} , Qifan Cui ², Xueying Bao ², Dong Gao ² and Chengfen Xing ^{2,*}

¹ National-Local Joint Engineering Laboratory for Energy Conservation in Chemical Process Integration and Resources Utilization, School of Chemical Engineering and Technology, Hebei University of Technology, Tianjin 300131, China; magang0629@163.com

² Key Laboratory of Hebei Province for Molecular Biophysics, Institute of Biophysics, Hebei University of Technology, Tianjin 300401, China; cuiqifan1228@163.com (Q.C.); XueyingBao2017@163.com (X.B.); gaodong@iccas.ac.cn (D.G.)

* Correspondence: qijunjie@hebut.edu.cn (J.Q.); xingc@hebut.edu.cn (C.X.); Tel./Fax: 86-22-60435642 (C.X.)

Received: 9 April 2020; Accepted: 7 May 2020; Published: 13 May 2020



Abstract: The multifunctional photothermal therapy (PTT) platform with the ability to selectively kill bacteria over mammalian cells has received widespread attention recently. Herein, we prepared graphene oxide-amino(polyethyleneglycol) (GO-PEG-NH₂) while using the hydrophobic interaction between heptadecyl end groups of 1,2-distearoyl-sn-glycero-3-phosphoethanolamine-N-[amino(polyethyleneglycol)] (DSPE-PEG-NH₂) and graphene oxide (GO). Based on GO-PEG-NH₂, the versatile PTT system was constructed with simultaneous selective recognition, capturing, and photothermal killing of bacteria. When the cells undergo bacterial infection, owing to the poly(ethylene glycol) (PEG) chains and positively charged amino groups, GO-PEG-NH₂ can specifically recognize and capture bacteria in the presence of cells. Meanwhile, the stable photothermal performance of GO-PEG-NH₂ enables the captured bacteria to be efficiently photothermally ablated upon the irradiation of 808 nm laser. Besides, the GO-PEG-NH₂ is highly stable in various biological media and it exhibits low cytotoxicity, suggesting that it holds great promise for biological applications. This work provides new insight into graphene-based materials as a PTT agent for the development of new therapeutic platforms.

Keywords: photothermal therapy (PTT); graphene oxide (GO); selective recognition and capturing; antibacterial

1. Introduction

The appearance of antibiotic resistance to pathogen bacteria is one of the major challenges in the global health field [1]. As an alternative approach, nanomaterials absorbing a specific wavelength of light have been exploited for the treatment of bacterial infections. Photothermal therapy (PTT) and photodynamic therapy (PDT) have attracted significant attention in recent years as photo-triggered antibacterial methods [2–7]. Unlike target-specific antibiotics, PTT and PDT are broad-spectrum pathogen killing methods that prevent the generation of specific resistant strains [8–11]. Recently, a great deal of pathogen killing systems has been explored, and multiantibiotic resistant bacteria can be easily killed by photo-triggered antibacterial methods [12–15]. However, the infection of mammalian hosts by pathogens often leads to the coexistence of both bacteria and cells. Hence, how to selectively kill bacteria in the presence of mammalian cells has become a research hotspot. Wang and co-workers have synthesized a water-soluble cationic poly(p-phenylene vinylene) derivative (PPV-1) containing Oligo(ethylene glycol) (OEG) side chain and quaternary ammonium (QA) groups, and pathogenic

bacteria are killed in the presence of cells by the dark-toxic QA group and the light-toxic PPV-1 main backbone to produce Reactive Oxygen Species (ROS) under white light [16]. Liu and co-workers have designed a multifunctional aggregation-induced emission-zinc(II)-diamine (AIE-ZnDPA) probe while using a positively charged zinc(II)-difunctional amine (ZnDPA) as a ligand to selectively target negatively charged bacterial membranes via electrostatic interaction. The positively charged ZnDPA groups killed pathogenic bacteria to depolarize the bacterial membrane and phototoxicity through the generation of ROS [17]. The above strategies all utilize photosensitizers (PSs) to generate ROS upon light irradiation to kill bacteria. PTT is another alternative approach to treat against bacteria that usually can lead to thermal ablation of microorganisms and cells by using near infrared (NIR) light to transform optical energy into heat [4,8,18–20]. Besides, PTT also has the advantages of simplicity, non-invasiveness, safety, and strong tissue penetration [21]. Zhang and co-workers have designed a supramolecular complex (CPPDI) by a perylene diimide derivative (PPDI) and cucurbit [7] uril (CB [7]) through host-guest interactions. CPPDI could be triggered into CPPDI radical anions in situ by anaerobic bacteria (such as *E. coli*), which was used in photothermal therapy under near-infrared radiation in order to achieve selective killing of bacteria [22]. Although some progress has been made in photothermal materials with selective antibacterial capabilities, developing novel photothermal agents with excellent selectivity toward bacteria and cells is still imperative. Based on this conception, we try to use PTT to achieve the selective capture and killing of bacteria over mammalian cells.

There are many types of photothermal conversion materials due to the tremendous potential of photothermal therapy applications [23,24], including precious metal nanomaterials [25], carbon nanomaterials [26,27], and transition metal dichalcogenides nanomaterials [28], have been explored for PTT in recent years. Graphene is a two-dimensional (2D) carbon nanomaterial that is composed of carbon atoms with sp^2 hybrid orbital hexagonal honeycomb lattice [5,29,30]. Graphene oxide (GO) and reduced graphene oxide (rGO) have been extensively used in various fields because of their impressive physical and chemical properties [31–36]. For example, the diverse defects and chemical functionalities on the graphene layers can catalyze reactions, while graphene can be used as a carrier for the catalytic reaction [37–39]. Besides, carbon nanomaterials such as graphene oxide have proven to be very promising nano weapons against multi-drug resistant bacteria [40,41]. Absorbing light irradiation can enhance the antibacterial properties of carbon nanomaterials against multidrug-resistant pathogens [42–44]. GO is an excellent PTT photothermal material with high photothermal conversion efficiency, high stability, and good biocompatibility [21,45–49].

In this work, we designed a DSPE-PEG-NH₂ (one end of DSPE-PEG-NH₂ is a hydrophobic structure 1,2-distearoyl-sn-glycero-3-phosphoethanolamine, and the other end is an amino-terminated PEG chain) modified GO composite (GO-PEG-NH₂) [50–52]. The cell wall of bacteria is mainly made of peptidoglycan and acid polysaccharide, which exhibits a large amount of net negative charges on the membrane surface. Under physiological conditions, mammalian cell membranes are nearly neutral with only a small quantity of negative charge. Therefore, the amino group of GO-PEG-NH₂ can be bound to a negatively charged bacterial membrane by electrostatic driving forces, and the presence of a PEG chain can also reduce the non-specific adsorption of cell surface proteins. The flexibility of the main polyether chain is responsible for these properties in this process [16,53]. At the same time, as a photothermal conversion material, GO can thermally ablate bacteria that are adsorbed on the surface of GO-PEG-NH₂ composite under 808 nm laser irradiation.

The most attractive finding of this work is that we prepared GO-PEG-NH₂ in an uncomplicated way to selectively identify and capture pathogenic bacteria and simultaneously kill pathogenic bacteria by photothermal. In addition, GO-PEG-NH₂ is found to be a green broad-spectrum antibacterial material, with little bacterial resistance and a tolerable cytotoxic effect on mammalian cells.

2. Materials and Methods

2.1. Reagents and Equipment

Graphene oxide (GO, Product code G139803) was purchased from Shanghai Aladdin Biotechnology Co., Ltd. (Shanghai, China). 1,2-distearoyl-sn-glycero-3-phosphoethanolamine-N-[methoxy(polyethyleneglycol)-2000(ammonium salt) (DSPE-PEG2000-NH₂) were purchased from Ananti Polar Lipids, Inc. (Beijing, China). Fetal bovine serum (FBS) was obtained from Sijiqing Biological Engineering Materials (Hangzhou, China). RPMR-1640 was purchased from Solarbio (Beijing, China). Isopropyl-beta-D-thiogalactopyranoside (IPTG) was purchased from Amresco Inc. (Houston, TX, USA). The human acute lymphoblastic leukemia cells (CCRF-CEM) were obtained from the Cell Bank of the Committee of Culture Collection of the Chinese Academy of Sciences (Shanghai, China).

A Malvern Nano-ZS90 (Malvern Inc., Malvern, UK) provided average particle sizes. The ultraviolet (UV)-visible light (vis) absorption values were taken on a Shimadzu UV-1800 UV-vis spectrophotometer (Shimadzu, Kyoto, Japan). The 808 nm laser was obtained from a Hi-Tech high power laser generator (Beijing, China). The absorbance for methylthiazolyl-diphenyl-tetrazolium bromide (MTT) analysis was taken on a SpectraMax i3 (Molecular Devices Inc., San Francisco, CA, USA) at a wavelength of 520 nm. Fluorescence imaging was recorded on a confocal laser scanning microscope (CLSM, Leica, Weztlar, Germany).

2.2. Synthesis of GO-PEG-NH₂

GO was sonicated for 2 h with an ultrasonic cell disrupter, and then centrifuged at 15,000 rpm for 10 min. DSPE-PEG2000-NH₂ (5 mg) and GO (2 mg/mL 0.5 mL) with a mass ratio of 5:1 were dispersed in 1 mL Tetrahydrofuran (THF) and sonicated for 30 min. The resulted material was added dropwise to 4 mL of ultrapure water and then stirred at 450 rpm for 12 h. The larger particle sizes of GO-PEG-NH₂ were removed by centrifugation (3000 rpm for 10 min.). Small molecules were removed by dialysis, and unreacted starting materials were removed by ultrafiltration.

2.3. Preparation of Bacterial Solutions

A single colony of *Escherichia coli* (*E. coli*) on a solid Luria Broth (LB) agar plate was picked and transferred to 7 mL liquid LB culture medium and then grown overnight at 37 °C. A certain volume of the bacterial liquid was taken, and the bacteria were harvested by centrifugation (7500 rpm for 5 min.) and washed three times with phosphate-buffered saline (PBS, 10 mM, pH = 7.4). Finally, the obtained bacteria were resuspended in PBS and diluted to an optical density of 1.0 (OD₆₀₀ = 1.0) at 600 nm. As for *Staphylococcus aureus* (*S. aureus*), the experimental conditions and operations were identical to that of *E. coli*.

2.4. Cell Culture

CCRF-CEM cells (suspension cells) were cultured in RPMI-1640 medium that was supplied with 15% fetal bovine serum (FBS). A certain amount of the culture solution was added to a 50 mL cell culture flask and then cultured at 37 °C in a humidified atmosphere containing 5% CO₂. CCRF-CEM should be mixed with the cell culture medium in the course of the passage, and half of the culture solution should be discarded, and fresh RPMI-1640 medium should be added. When the cells are in good condition, it requires replacing by liquid replacement every other day.

2.5. Cytotoxicity Assay

In this experiment, the cytotoxicity analysis of GO-PEG-NH₂ was evaluated by the standard MTT assay. The CCRF-CEM cells were seeded in 96-well plates at a density of $1 \times 10^4 \sim 3 \times 10^4$ cells/well and then incubated overnight. Various concentrations of GO-PEG-NH₂ in fresh culture medium were

added into the cells. The cells were incubated at 37 °C for 24 h. The cells were washed with PBS. Unbound GO-PEG-NH₂ was removed by centrifugation (300 rpm for 5 min.), and then 200 µL of MTT (0.5 mg/mL, dissolved in cell culture medium without bovine serum) was added to each well and incubated for 4 h at 37 °C. The supernatant was removed by centrifugation (300 rpm for 10 min.), and 150 µL of Dimethyl sulfoxide (DMSO) was added to each well and shaken in a shaker for 10 min. to dissolve the produced formazan. The absorbance values of the wells were read with a microplate reader at 520 nm. The untreated cells served as the control and their viability was set as 100%.

2.6. ζ Potential Measurements

CCRF-CEM, *E. coli* and *S. aureus* in PBS were incubated with 50 µg/mL GO-PEG-NH₂ at 37 °C for 30 min., respectively. Unbound GO-PEG-NH₂ was removed by centrifugation (500 rpm 5 min. for CCRF-CEM; 1500 rpm 5 min. for bacteria), and the bottoms pellet was resuspended in PBS. As a control, bacteria and cells without GO-PEG-NH₂ were incubated under the same conditions. DLS measured the potential values of the cell suspension and the bacterial suspension.

2.7. Antibacterial Experiments

The antibacterial test was evaluated with the colony counting method [54,55]. *E. coli* and *S. aureus* bacterial suspensions with an OD₆₀₀ of 1.0 were incubated with different concentrations of GO-PEG-NH₂ under dark at 37 °C for 1 h. The supernatant was removed by centrifugation (1500 rpm for 5 min.), the sediment was collected, and the bacteria were resuspended in PBS. Subsequently, 200 µL of the bacterial suspension was added to a 96-well U-shaped cell culture plate and the bacterial suspension was irradiated with an 808 nm laser at an optical density of 1.5 W/cm² for 5 min. After irradiation, the bacterial suspensions were serially diluted 1.0 to 1 × 10⁴ fold with PBS. A 10 µL portion of the diluted bacterial suspension was spread on the solid LB agar plate and then incubated at 37 °C for 12 h. The number of colonies was counted using the colony counting method and the bacteria survival rates were determined from CFU counting on the solid LB agar plate with the control under dark without GO-PEG-NH₂ treatment. For the control under dark, the irradiation step was replaced by incubation under dark for 5 min.

2.8. Scanning Electron Microscopy (SEM) Characterization

SEM was used to observe the morphological changes of bacteria [16,17]. *E. coli* and *S. aureus* bacterial suspensions with an OD₆₀₀ of 1.0 were incubated with GO-PEG-NH₂ (50 µg/mL) under dark at 37 °C for 30 min, as described in antibacterial experiments. The concentration of GO-PEG-NH₂ is determined by a standard curve (Figure S1). After irradiation, the bacteria were harvested by centrifugation, and immediately transferred to glutaraldehyde (2.5%) in PBS solution and fixed at 4 °C for 4 h. The bacteria were then collected by centrifugation and washed three times with sterile water. Dehydration was carried out sequentially with 10%, 30%, 50%, 70%, 90%, and 100% ethanol solution. Finally, the bacteria in 100% ethanol solution were added dropwise to clean silicon slices and then dried under vacuum overnight. The specimens were coated with platinum before SEM studies.

2.9. *E. coli* was Induced by IPTG to Express Recombinant Green Fluorescent Protein

A single colony of *E. coli* (Gram-negative) on a solid Luria Broth (LB) agar plate was picked and transferred to 10 mL liquid LB culture medium and grown at 37 °C for 20 h. Subsequently, IPTG (1 mM) was added to the *E. coli* solution in the log phase. After that, *E. coli* was continued at 37 °C for 4 h. A certain volume of the bacterial liquid was taken, and the bacteria were harvested by centrifugation (7500 rpm for 5 min.) and then washed three times with phosphate-buffered saline (PBS, 10 mM, pH = 7.4). Finally, the obtained bacteria were resuspended in PBS and then diluted to an optical density of 1.0 (OD₆₀₀ = 1.0) at 600 nm.

2.10. Confocal Laser Scanning Microscopy (CLSM) Characterization

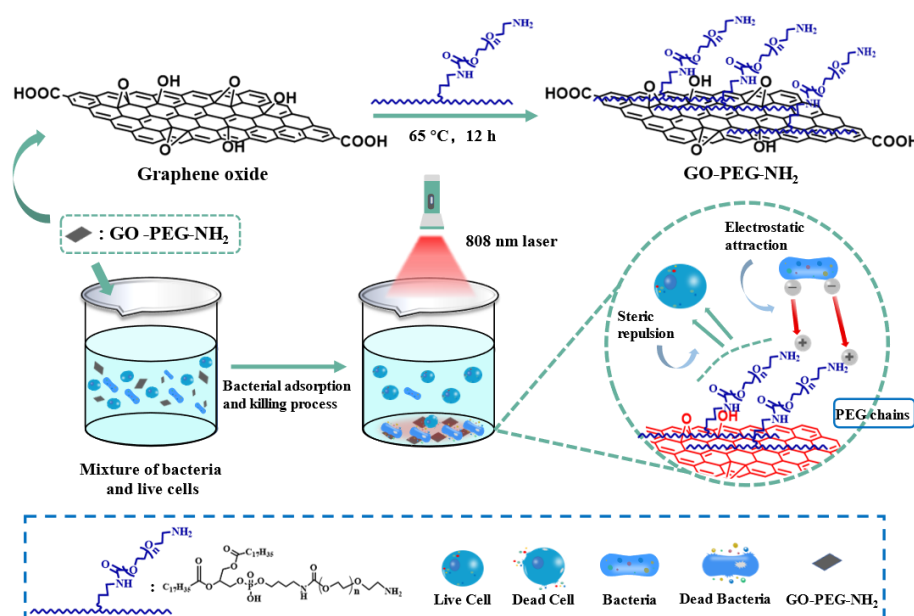
The prepared *E. coli* and CCRF-CEM cell solutions were incubated with GO-PEG-NH₂ for 30 min. at 37 °C under the dark, respectively. Afterwards, 10 µL of the mixed suspension was added to the alcohol-treated glass slides and gently fixed with clean coverslips. Confocal laser scanning microscopy imaged the samples. The excitation wavelength is 488 nm.

For confocal images of the suspended cells and bacteria mixtures, the prepared *E. coli* and CCRF-CEM cell solutions were mixed and then incubated with 50 µg/mL GO-PEG-NH₂ at 37 °C for 30 (and 60) min. under the dark. Individual aliquots of 10 µL of the prepared suspension were spotted on alcohol pretreated glass slides and then immobilized by the coverslips. Confocal laser scanning microscopy imaged the samples. The excitation wavelength is 488 nm. The fluorescence of *E. coli* is highlighted in green.

3. Results and Discussion

3.1. Preparation and Mechanism of GO-PEG-NH₂

Scheme 1 shows the mechanism for recognition, capturing, and photothermal killing of bacteria over mammalian cells. DSPE-PEG-NH₂ can be tightly attached to GO through hydrophobic interactions between heptadecyl end groups and GO, yielding the surface of GO film by amino groups and PEG chains [26,50,56,57]. The membrane potential difference between bacteria and cells results in a competitive attraction of GO-PEG-NH₂ to bacteria. The accumulation of bacteria on the surface of GO-PEG-NH₂ by electrostatic interaction leads to the sedimentation of bacteria and GO-PEG-NH₂. The GO converts light energy into heat upon irradiation under NIR light (808 nm) with the optical density of 1.5 W/cm², which causes the thermal ablation of the bacteria.



Scheme 1. Schematic representation of the fabrication process of graphene oxide-amino(polyethyleneglycol) (GO-PEG-NH₂) and GO-PEG-NH₂ for the selective recognition, capturing, and photothermal killing of bacteria over mammalian cells. The sizes of cells and bacteria are not drawn to scale.

3.2. Characterization of Structure and Photothermal Properties

The morphology of GO-PEG-NH₂ was characterized by atomic force microscope (AFM), as shown in Figure 1a [39]. GO-PEG-NH₂ was almost a single-layered sheet with an average topographic height

of ~ 1.75 nm (Figure 1b). When compared to GO, the average topological height of GO-PEG-NH₂ has increased by a certain amount (from ~ 1.37 nm to ~ 1.75 nm, Figure S2a,b), indicating that many polymer chains have been wrapped around the surface of the GO sheets. It has been documented that the cell membrane of bacteria is effectively destroyed by direct contact between the bacteria and the very sharp edges of graphene, resulting in the inactivation of bacteria by graphene [58,59]. The ultrasonic vibration and mechanical stirring may remove the sharp edges of GO during the preparation process [60]. The edges of GO sheets are very sharp, while the edges of GO-PEG-NH₂ are smoother and rounder, which may enhance biocompatibility, as shown in the AFM charts. The more rounded edges reduce the physical damage to the cell membrane by GO-PEG-NH₂. The SEM image of GO-PEG-NH₂ exhibits a sheet-like structure with a smooth surface, small thickness, and small wrinkles at the edges, as illustrated in Figure S2f. Dynamic light scattering (DLS) shows that the average hydrodynamic size of GO-PEG-NH₂ was smaller than GO (from 956.90 ± 17.01 nm to 459.03 ± 10.54 nm, Figure S2c,d), which might be caused by ultrasonic vibration during the preparation process. The physicochemical characteristics of graphene, such as the lateral size, surface charges, and surface functional groups, can have a significant impact on its biocompatibility. The reduction of lateral size can reduce the threat of GO-PEG-NH₂ to the cells in a mixed state to a certain extent [12,61]. The potential of GO-PEG-NH₂ is -4.27 ± 0.52 mV, which became more cationic after the functionalization of DSPE-PEG-NH₂ (Table 1), indicating that positively charged amino groups successfully bind to the surface of GO-PEG-NH₂. As an experiment to verify the stability of GO-PEG-NH₂, it was incubated in various biological media (water, PBS, RPMI-1640 medium, and fetal bovine serum) for 24 h (Figure S2e). The introduction of the PEG chain increases the hydrophilicity of GO-PEG-NH₂. Besides, the relatively small particle size of the GO-PEG-NH₂ composite also gives it better stability. The stability experiment shows the enormous potential of GO-PEG-NH₂ in biological applications.

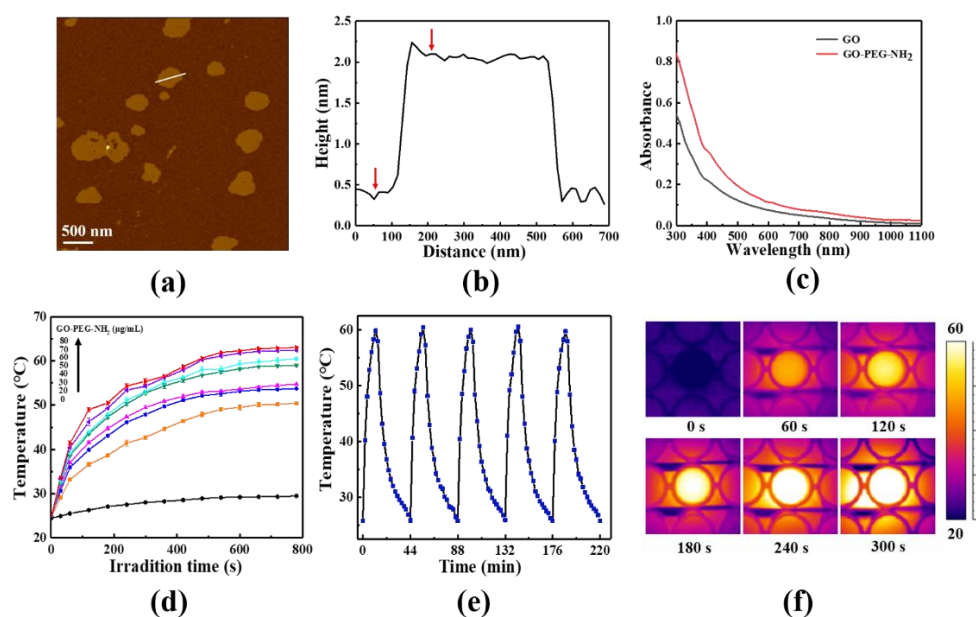


Figure 1. Characterization and photothermal performance of GO-PEG-NH₂. (a) AFM image of GO-PEG-NH₂ deposited on a mica substrate. (b) The height profile of the AFM image. The red arrows indicate the height difference. (c) UV-vis-NIR absorption spectrum of GO and GO-PEG-NH₂. (d) Temperature distribution of pure water and different concentrations of GO-PEG-NH₂ aqueous solution under 808 nm laser irradiation. Different concentrations of GO-PEG-NH₂ are distinguished by colored lines. (e) Photothermal conversion cycling test of GO-PEG-NH₂ aqueous solution under five cycles of 808 nm laser irradiation (1.5 W/cm^2). (f) Infrared thermal image of GO-PEG-NH₂ aqueous solution ($50 \mu\text{g/mL}$) under 808 nm laser irradiation.

Table 1. ζ potentials of GO, GO-PEG-NH₂, *E. coli*, *S. aureus*, and CCRF-CEM incubation with and without GO-PEG-NH₂.

Species	ζ Potential/mV	
	GO-PEG-NH ₂ (–)	GO-PEG-NH ₂ (+)
GO	–41.30 ± 0.36	–
GO-PEG-NH ₂	–4.27 ± 0.52	–
<i>E. coli</i>	–51.83 ± 0.61	–14.60 ± 0.79
<i>S. aureus</i>	–34.63 ± 0.12	–25.70 ± 0.91
CCRF-CEM	–11.70 ± 0.16	–10.80 ± 0.29

The absorption spectrum of GO-PEG-NH₂ shows a broad absorption band from the ultraviolet (UV) to the NIR regions, which are similar to GO (Figure 1c). The modification of DSPE-PEG-NH₂ did not destroy the original structure of GO. The heating curves of different concentrations of GO-PEG-NH₂ aqueous solution under 808 nm laser irradiation were measured to further evaluate the photothermal properties of GO-PEG-NH₂. The temperatures of GO-PEG-NH₂ aqueous solutions increased rapidly with the extending irradiation time and the increasing concentration of GO-PEG-NH₂, as shown in Figure 1d. It is worth noting that, after 5 min. of irradiation, the temperature of GO-PEG-NH₂ aqueous solution can be increased to 55 °C at the concentration of 50 µg/mL, which is sufficient for the bacteria to ablate. The photothermal conversion cycling experiment showed that the photothermal effect of GO-PEG-NH₂ was almost unchanged during the heating process after five cycles of irradiation, which proved that it has good photothermal stability (Figure 1e). The infrared thermal images of 50 µg/mL GO-PEG-NH₂ aqueous solution under 808 nm laser irradiation was collected, and the infrared thermal images were consistent with the photothermal heating curves (Figure 1f). Strong photothermal properties make GO-PEG-NH₂ an excellent photothermal agent.

3.3. Selective Adsorption of GO-PEG-NH₂

Confocal laser scanning microscopy (CLSM) was used to directly visualize the selective association of GO-PEG-NH₂ in a mixture of live cells and bacteria to verify that GO-PEG-NH₂ could selectively target bacteria over mammalian cells. Gram-positive bacteria (*Staphylococcus aureus*) and Gram-negative bacteria (*Escherichia coli*) were used as representative strains in order to verify the selective association of GO-PEG-NH₂ with bacteria. At the same time, the suspension of CCRF-CEM cells was selected for experimentation because it does not require trypsin digestion to avoid undesirable autofluorescence. Firstly, we used isopropyl- β -D-thiogalactoside (IPTG) to induce *E. coli* expression of EGFP as a marker to visualize the selective binding mechanism of GO-PEG-NH₂, and when considering the excellent fluorescence properties of enhanced green fluorescent protein (EGFP). When compared with other markers, EGFP has the advantages of small molecular weight, non-toxic effect in bacterial and eukaryotic cells, and stable fluorescence. Secondly, CLSM images of IPTG-induced *E. coli* and CCRF-CEM cells blended with GO-PEG-NH₂ treatment were obtained to validate our strategy. In subsequent experiments, *E. coli* and CCRF-CEM cells were mixed and incubated with GO-PEG-NH₂ at 37 °C for 30 min. The results showed that the bacteria were attached to GO-PEG-NH₂, while most of the cells were still in a freely dispersed state (Figure 2a,e). It should be pointed out that a small number of cells were also adsorbed by GO-PEG-NH₂. The probable reason is that part of the apoptosis exposes the phosphatidylserine (PS) in the inner leaflets of the plasma membrane, resulting in a large increase in the negative charge density on the cell membrane surface. After additional 30 min. incubation, the fluorescent image of the supernatant showed that only a small amount of bacteria was present and the cells were normally dispersed in the solution (Figure 2b,f).

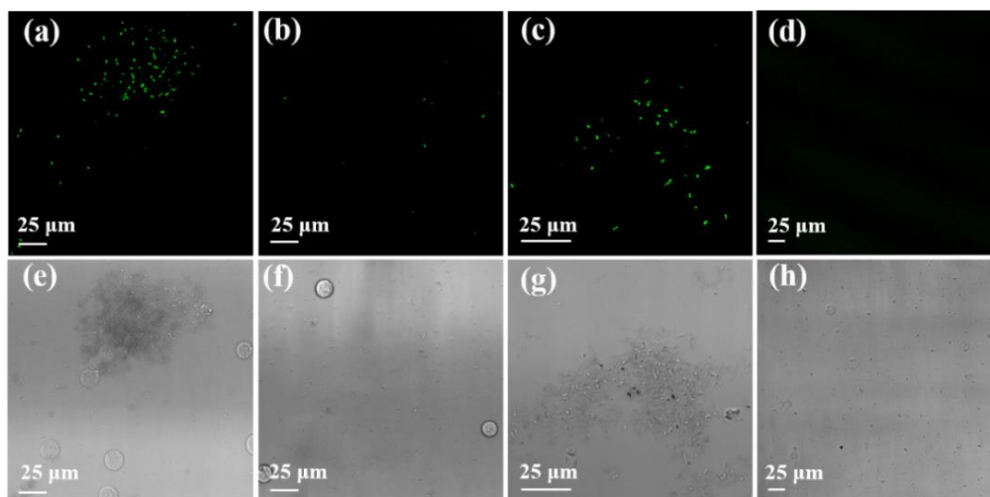


Figure 2. (a,e) Confocal laser scanning microscope (CLSM) images of isopropyl-beta-D-thiogalactopyranoside (IPTG)-induced *E. coli* and human acute lymphoblastic leukemia cells (CCRF-CEM) incubated with GO-PEG-NH₂ (50 μg/mL) for 30 min; (b,f) CLSM images of bright field and fluorescent images of the supernatant after incubation for 60 min. To further determine the selectivity of GO-PEG-NH₂ for bacteria, IPTG-induced *E. coli* and CCRF-CEM cells were incubated with GO-PEG-NH₂ at 37 °C for 30 min., respectively. (c,g) CLSM images of bacteria adsorbed on GO-PEG-NH₂; (d,h) The cells were incubated with GO-PEG-NH₂ for 30 min. and normally dispersed in the solution. The fluorescence of IPTG-induced *E. coli* is highlighted in green.

IPTG-induced *E. coli* and CCRF-CEM cells were incubated with GO-PEG-NH₂ at 37 °C for 30 min., respectively, to further determine the selectivity of GO-PEG-NH₂ for bacteria. Clear fluorescence images indicate that GO-PEG-NH₂ can be associated with bacteria (Figure 2c,g) without interacting with CCRF-CEM cells (Figure 2d,h). As a control, morphological images of bacteria and cells at the same concentration were collected, as shown in Figure S3, the observed cell and bacteria morphology keeps well and no characteristic changes were detected for the case of cells and bacteria untreated with GO-PEG-NH₂. All of the above data reveal the fact that GO-PEG-NH₂ can selectively bind to bacteria, but not to cells. The cell wall of bacteria is mainly made of peptidoglycan and acid polysaccharide, which exhibits a large amount of net negative charges on the membrane surface. In normal cells, PS is strictly confined in the inner leaflets of the plasma membrane, which results in its cell membrane being nearly neutral. Most importantly, the use of PEG to reduce protein adsorption and cell adhesion is well documented in the literature [16,53]. These factors determine that GO-PEG-NH₂ tends to bind to bacteria, but not to cells.

The interaction mechanism between GO-PEG-NH₂ and bacteria was analyzed by measuring the surface potential of bacteria and cells in order to further understand that GO-PEG-NH₂ can selectively recognize and capture bacteria. Table 1 summarizes the ζ potentials of *S. aureus*, *E. coli*, and CCRF-CEM incubated with and without GO-PEG-NH₂. The potentials of *E. coli* (from -51.83 ± 0.61 mV to -14.6 ± 0.79 mV) and *S. aureus* (from -34.63 ± 0.12 mV to -25.7 ± 0.91 mV) became more cationic after incubation with GO-PEG-NH₂, indicating that *E. coli* and *S. aureus* successfully bind to the surface of GO-PEG-NH₂. This is due to the active amino group on the surface of GO-PEG-NH₂ that can act as a “linker” between the material and bacteria through electrostatic attraction. The potential of CCRF-CEM cells (from -11.70 ± 0.16 mV to -10.8 ± 0.29 mV) does not change much before and after incubation with GO-PEG-NH₂. Bacteria carry more negative charges than the surface of the cells, which provide the most direct driving force for selective association in a mixed system, as mentioned above. Therefore, interaction between bacteria and GO-PEG-NH₂ might be determined by the localized interaction between positively charged amino groups and negatively charged bacterial surfaces. The fluorescence image shows the fact that CCRF-CEM cells do not easily bind to GO-PEG-NH₂ and, therefore, the ζ

potentials remain almost unchanged. The results of the potential test are in line with the conclusions obtained by CLSM.

3.4. Antibacterial Ability

Based on the selective affinity of GO-PEG-NH₂ to bacteria and its potential antibacterial activity, the antibacterial activity of GO-PEG-NH₂ was subsequently studied. The MTT assay was used to analyze mammalian cells viability and the antibacterial test was evaluated with the colony counting method. Cell viability slightly decreases with the increase of GO-PEG-NH₂ concentration, as illustrated in Figure 3a. However, cell viability still keeps at about 90%, even when the concentration reaches 70 µg/mL. That is to say, the cell viability of CCRF-CEM did not change significantly as the concentration of GO-PEG-NH₂ increased, indicating that GO-PEG-NH₂ had no obvious toxicity to cells. Good stability and low biotoxicity in biological media make GO-PEG-NH₂ have great potential for biological applications. For *S. aureus* and *E. coli*, the traditional plate counting method first studied the sterilization efficiency of GO-PEG-NH₂ with different concentrations. From the histogram displayed in Figure 3b, the sterilization efficiency rapidly increased with the increasing concentration of GO-PEG-NH₂. Impressively, when the concentration of GO-PEG-NH₂ is 30 µg/mL, the killing efficiency could reach 80%. Under the condition of 808 nm laser irradiation, the survival rate of bacteria could reach more than 90%, as shown in Figure 3c. At the same time, GO-PEG-NH₂ also has a certain killing effect on bacteria under dark condition. This is due to the antibacterial properties of graphene oxide itself, and the positively charged GO-PEG-NH₂ group can effectively depolarize the bacterial membrane. After the 808 nm laser was irradiated for 5 min., the temperature of the solution had risen to 55 °C, and the colony counting showed that the killing efficiency of GO-PEG-NH₂ could reach more than 99%. Under NIR irradiation, electrons gain energy from the ground state and transition to an excited state with higher energy. Unstable electrons release thermal energy in the process of returning to a low energy state, which is the most direct cause of bacterial photothermal ablation. The gel images of bacteria and the colony count statistics of the plate counting method are given in the supporting information (Figure S4 and Tables S1–S3).

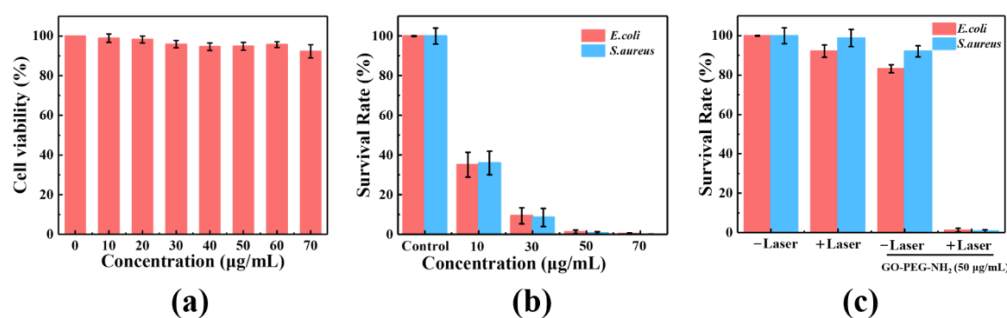


Figure 3. (a) Cell viability of CCRF-CEM cells after incubation with various concentrations of GO-PEG-NH₂ for 24 h. (b) Biocidal activity toward *E. coli* and *S. aureus*. Relative survival of bacteria after different concentrations of GO-PEG-NH₂ photothermal antibacterial experiments under 808 nm laser (1.5 W/cm²) for 5 min. (c) Relative survival rate of bacteria under four conditions when the concentration of GO-PEG-NH₂ was 50 µg/mL. Additionally, the effects of 808 nm laser and GO-PEG-NH₂ were determined.

Field-emission SEM was used to observe the morphological changes of bacteria in order to visually understand the damage of GO-PEG-NH₂ to bacteria before and after 808 nm laser irradiation. For *S. aureus* and *E. coli*, a control group without GO-PEG-NH₂, the bacteria were intact, the surface was smooth, and the edges were visible (Figure 4a,d). When GO-PEG-NH₂ was added under the dark, the bacteria undergo a certain degree of agglomeration, and the surface of the bacterial membrane was damaged and collapsed (Figure 4b,e). This is consistent with the views stated above. After the 808 nm laser irradiation, the bacterial membrane was completely broken and the membrane was

fused (Figure 4c,f). The direct information from SEM images clearly shows the damage caused by GO-PEG-NH₂ on bacterial membrane under both dark and 808 nm laser irradiation.

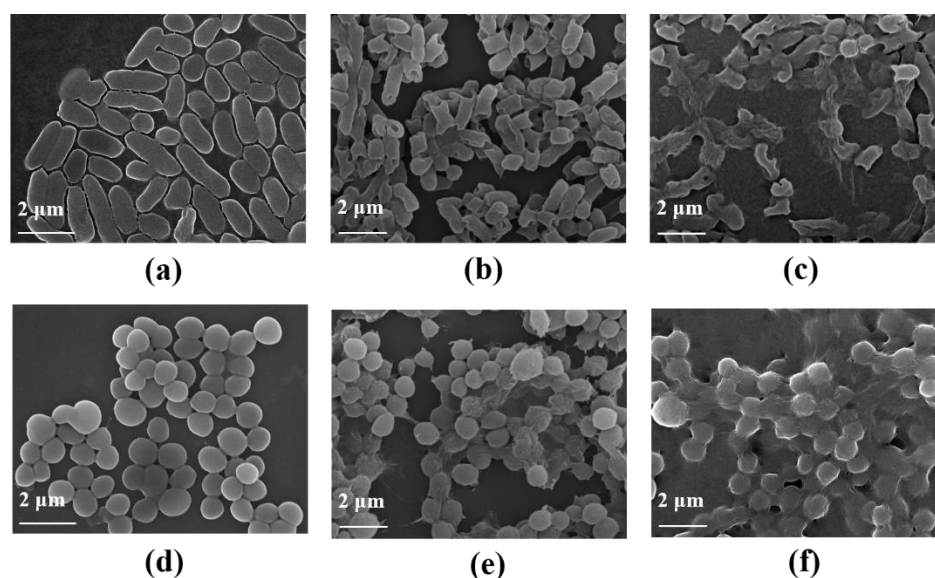


Figure 4. Morphologies of (a–c) *E. coli* and (d–f) *S. aureus* upon incubation with GO-PEG-NH₂: (a,d) without GO-PEG-NH₂ under dark; (b,e) with GO-PEG-NH₂ (50 µg/mL) under dark; and, (c,f) with GO-PEG-NH₂ (50 µg/mL) and 808 nm laser irradiation (1.5 W/cm² for 5 min.).

4. Conclusions

In summary, we have reported the multifunctional photothermal material GO-PEG-NH₂ for the selective recognition, capturing, and photothermal killing of bacteria over mammalian cells. When the cells undergo bacterial infection, the higher negative charge density on the bacterial surface provides an inherent electrostatic driving force for GO-PEG-NH₂, which can competitively bind to bacteria, but not to cells. Therefore, the bacteria-attractive GO-PEG-NH₂ provides a simple method for differentiating bacteria and cells. At the same time, GO-PEG-NH₂, as an excellent photothermal agent, can effectively kill bacteria. The antimicrobial activity of GO-PEG-NH₂ arises from two parts: the thermal energy generated by the 808 nm laser irradiation and the toxicity from positively charged amino groups to depolarize the bacterial membrane. Besides, the GO-PEG-NH₂ is highly stable in various biological media and it exhibits low cytotoxicity, suggesting that it holds great promise for biological applications. In short, by combining the competitive bacteria adsorption property and the excellent antibacterial ability into a versatile system, this work provides new insight into graphene-based materials as a PTT agent for the development of new therapeutic platforms.

Supplementary Materials: The following are available online at <http://www.mdpi.com/2073-4360/12/5/1116/s1>. Figure S1: Standard curve of GO-PEG-NH₂ in PBS. Figure S2: (a) AFM image of GO deposited on mica substrate. (b) The height profile of the AFM image. (c) Hydrodynamic diameter of GO measured by DLS. (d) Hydrodynamic diameter of GO-PEG-NH₂ measured by DLS. (e) Photograph of GO-PEG-NH₂ dispersed in different culture media for 24 h. (f) SEM image of GO-PEG-NH₂. Figure S3: CLSM images of (a, b) *E. coli*, (c, d) CCRF-CEM. Figure S4: Gel imaging of *E. coli* and *S. aureus* colonies. (a, e) Plate photographs of the *E. coli* and *S. aureus* LB agar plate without GO-PEG-NH₂ under dark. (b, f) Plate photographs for *E. coli* and *S. aureus* LB agar plate supplemented with GO-PEG-NH₂ (50 µg/mL) under dark. (c, g) Plate photographs for *E. coli* and *S. aureus* LB agar plate upon 808 nm laser irradiation (1.5 W/cm² for 5 min). (d, h) Plate photographs for *E. coli* and *S. aureus* LB agar plate supplemented with GO-PEG-NH₂ upon 808 nm laser irradiation. Table S1: Evaluation of *E. coli* colonies by plate counting method (The power density of the 808 nm laser is 1.5 W/cm², the irradiation time is 5 min, and the concentration of GO-PEG-NH₂ is 50 µg/mL). Table S2: Evaluation of *S. aureus* colonies by plate counting method (The power density of the 808 nm laser is 1.5 W/cm², the irradiation time is 5 min, and the concentration of GO-PEG-NH₂ is 50 µg/mL). Table S3: Evaluation of *S. aureus* and *E. coli* colonies by plate counting method (The power density of the 808 nm laser is 1.5 W/cm², and the irradiation time is 5 min).

Author Contributions: C.X. and J.Q. designed experiments and organized the manuscript; G.M. performed experimental part and analyzed data; X.B. and Q.C. performed experimental part; D.G. analyzed data. All authors have read and agreed to the published version of the manuscript.

Funding: National Natural Science Foundation of China (No.21574037, No.21773054 and No.51803046), the “100 Talents” Program of Hebei Province, China (No.E2014100004), the Natural Science Foundation of Hebei Province (No.B2017202051, E2015202073), the Program for Top 100 Innovative Talents in Colleges and Universities of Hebei Province (No.SLRC2017028), Foundation of Hebei Educational Committee (QN2014024).

Acknowledgments: The authors are grateful for the financial support of the National Natural Science Foundation of China (No.21574037, No.21773054 and No.51803046), the “100 Talents” Program of Hebei Province, China (No.E2014100004), the Natural Science Foundation of Hebei Province (No.B2017202051, E2015202073), the Program for Top 100 Innovative Talents in Colleges and Universities of Hebei Province (No.SLRC2017028), Foundation of Hebei Educational Committee (QN2014024).

Conflicts of Interest: The authors declare no conflict of interest.

References

1. Gallagher, L.A.; Shendure, J.; Manoil, C. Genome-scale identification of resistance functions in *Pseudomonas aeruginosa* using Tn-seq. *MBio* **2011**, *2*, e00315-10. [[CrossRef](#)] [[PubMed](#)]
2. Sortino, S. Photoactivated nanomaterials for biomedical release applications. *J. Mater. Chem.* **2012**, *22*, 301–318. [[CrossRef](#)]
3. Yhee, J.Y.; Koo, H.; Lee, D.E.; Choi, K.; Kwon, I.C.; Kim, K. Multifunctional Chitosan Nanoparticles for Tumor Imaging and Therapy. *Adv. Polym. Sci.* **2011**, *243*, 139–161.
4. Song, X.; Chen, Q.; Liu, Z. Recent advances in the development of organic photothermal nano-agents. *Nano Res.* **2014**, *8*, 340–354. [[CrossRef](#)]
5. Robinson, J.T.; Tabakman, S.M.; Liang, Y.; Wang, H.; Casalongue, H.S.; Vinh, D.; Dai, H. Ultrasmall reduced graphene oxide with high near-infrared absorbance for photothermal therapy. *J. Am. Chem. Soc.* **2011**, *133*, 6825–6831. [[CrossRef](#)] [[PubMed](#)]
6. Yang, H.; Mao, H.; Wan, Z.; Zhu, A.; Guo, M.; Li, Y.; Li, X.; Wan, J.; Yang, X.; Shuai, X.; et al. Micelles assembled with carbocyanine dyes for theranostic near-infrared fluorescent cancer imaging and photothermal therapy. *Biomaterials* **2013**, *34*, 9124–9133. [[CrossRef](#)]
7. Cheng, L.; Wang, C.; Feng, L.; Yang, K.; Liu, Z. Functional nanomaterials for phototherapies of cancer. *Chem. Rev.* **2014**, *114*, 10869–10939. [[CrossRef](#)]
8. Kim, H.; Chung, K.; Lee, S.; Kim, D.H.; Lee, H. Near-infrared light-responsive nanomaterials for cancer theranostics. *Wiley Interdiscip. Rev. Nanomed. Nanobiotechnol.* **2016**, *8*, 23–45. [[CrossRef](#)]
9. Liu, S.; Yuan, H.; Bai, H.; Zhang, P.; Lv, F.; Liu, L.; Dai, Z.; Bao, J.; Wang, S. Electrochemiluminescence for Electric-Driven Antibacterial Therapeutics. *J. Am. Chem. Soc.* **2018**, *140*, 2284–2291. [[CrossRef](#)]
10. Bai, H.; Yuan, H.; Nie, C.; Wang, B.; Lv, F.; Liu, L.; Wang, S. A Supramolecular Antibiotic Switch for Antibacterial Regulation. *Angew. Chem. Int. Ed. Engl.* **2015**, *54*, 13208–13213. [[CrossRef](#)]
11. Xing, C.; Xu, Q.; Tang, H.; Liu, L.; Wang, S. Conjugated Polymer/Porphyrin Complexes for Efficient Energy Transfer and Improving Light-Activated Antibacterial Activity. *J. Am. Chem. Soc.* **2009**, *131*, 13117–13124. [[CrossRef](#)] [[PubMed](#)]
12. Ji, H.; Sun, H.; Qu, X. Antibacterial applications of graphene-based nanomaterials: Recent achievements and challenges. *Adv. Drug Deliv. Rev.* **2016**, *105*, 176–189. [[CrossRef](#)] [[PubMed](#)]
13. Yang, J.; Zhang, X.; Ma, Y.H.; Gao, G.; Chen, X.; Jia, H.R.; Li, Y.H.; Chen, Z.; Wu, F.G. Carbon Dot-Based Platform for Simultaneous Bacterial Distinguishment and Antibacterial Applications. *ACS Appl. Mater. Interfaces* **2016**, *8*, 32170–32181. [[CrossRef](#)] [[PubMed](#)]
14. Zhao, L.; Xing, Y.; Wang, R.; Yu, F.; Yu, F. Self-Assembled Nanomaterials for Enhanced Phototherapy of Cancer. *ACS Appl. Bio Mater.* **2019**, *3*, 86–106. [[CrossRef](#)]
15. Peng, R.; Luo, Y.; Cui, Q.; Wang, J.; Li, L. Near-Infrared Conjugated Oligomer for Effective Killing of Bacteria through Combination of Photodynamic and Photothermal Treatment. *ACS Appl. Bio Mater.* **2020**. [[CrossRef](#)]
16. Zhu, C.; Yang, Q.; Liu, L.; Lv, F.; Li, S.; Yang, G.; Wang, S. Multifunctional cationic poly(p-phenylene vinylene) polyelectrolytes for selective recognition, imaging, and killing of bacteria over mammalian cells. *Adv. Mater.* **2011**, *23*, 4805–4810. [[CrossRef](#)]

17. Gao, M.; Hu, Q.; Feng, G.; Tomczak, N.; Liu, R.; Xing, B.; Tang, B.Z.; Liu, B. A multifunctional probe with aggregation-induced emission characteristics for selective fluorescence imaging and photodynamic killing of bacteria over mammalian cells. *Adv. Healthc Mater.* **2015**, *4*, 659–663. [[CrossRef](#)]
18. Chen, Q.; Wen, J.; Li, H.; Xu, Y.; Liu, F.; Sun, S. Recent advances in different modal imaging-guided photothermal therapy. *Biomaterials* **2016**, *106*, 144–166. [[CrossRef](#)]
19. Gai, S.; Yang, G.; Yang, P.; He, F.; Lin, J.; Jin, D.; Xing, B. Recent advances in functional nanomaterials for light-triggered cancer therapy. *Nano Today* **2018**, *19*, 146–187. [[CrossRef](#)]
20. Liu, Y.; Bhattarai, P.; Dai, Z.; Chen, X. Photothermal therapy and photoacoustic imaging via nanotheranostics in fighting cancer. *Chem. Soc. Rev.* **2019**, *48*, 2053–2108. [[CrossRef](#)]
21. Yang, K.; Zhang, S.; Zhang, G.; Sun, X.; Lee, S.T.; Liu, Z. Graphene in mice: Ultrahigh in vivo tumor uptake and efficient photothermal therapy. *Nano Lett.* **2010**, *10*, 3318–3323. [[CrossRef](#)] [[PubMed](#)]
22. Yang, Y.; He, P.; Wang, Y.; Bai, H.; Wang, S.; Xu, J.F.; Zhang, X. Supramolecular Radical Anions Triggered by Bacteria In Situ for Selective Photothermal Therapy. *Angew. Chem. Int. Ed. Engl.* **2017**, *56*, 16239–16242. [[CrossRef](#)] [[PubMed](#)]
23. Tao, W.; Ji, X.; Xu, X.; Islam, M.A.; Li, Z.; Chen, S.; Saw, P.E.; Zhang, H.; Bharwani, Z.; Guo, Z.; et al. Antimonene Quantum Dots: Synthesis and Application as Near-Infrared Photothermal Agents for Effective Cancer Therapy. *Angew. Chem. Int. Ed. Engl.* **2017**, *56*, 11896–11900. [[CrossRef](#)] [[PubMed](#)]
24. Jaque, D.; Martinez Maestro, L.; del Rosal, B.; Haro-Gonzalez, P.; Benayas, A.; Plaza, J.L.; Martin Rodriguez, E.; Garcia Sole, J. Nanoparticles for photothermal therapies. *Nanoscale* **2014**, *6*, 9494–9530. [[CrossRef](#)] [[PubMed](#)]
25. Wang, B.K.; Yu, X.F.; Wang, J.H.; Li, Z.B.; Li, P.H.; Wang, H.; Song, L.; Chu, P.K.; Li, C. Gold-nanorods-siRNA nanoplex for improved photothermal therapy by gene silencing. *Biomaterials* **2016**, *78*, 27–39. [[CrossRef](#)] [[PubMed](#)]
26. Li, S.; Chen, Y.; Liu, H.; Wang, Y.; Liu, L.; Lv, F.; Li, Y.; Wang, S. Graphdiyne Materials as Nanotransducer for in Vivo Photoacoustic Imaging and Photothermal Therapy of Tumor. *Chem. Mater.* **2017**, *29*, 6087–6094. [[CrossRef](#)]
27. Shi, J.; Wang, L.; Zhang, J.; Ma, R.; Gao, J.; Liu, Y.; Zhang, C.; Zhang, Z. A tumor-targeting near-infrared laser-triggered drug delivery system based on GO@Ag nanoparticles for chemo-photothermal therapy and X-ray imaging. *Biomaterials* **2014**, *35*, 5847–5861. [[CrossRef](#)]
28. Cheng, L.; Liu, J.; Gu, X.; Gong, H.; Shi, X.; Liu, T.; Wang, C.; Wang, X.; Liu, G.; Xing, H.; et al. PEGylated WS(2) nanosheets as a multifunctional theranostic agent for in vivo dual-modal CT/photoacoustic imaging guided photothermal therapy. *Adv. Mater.* **2014**, *26*, 1886–1893. [[CrossRef](#)]
29. Zhu, Y.; Murali, S.; Cai, W.; Li, X.; Suk, J.W.; Potts, J.R.; Ruoff, R.S. Graphene and graphene oxide: Synthesis, properties, and applications. *Adv. Mater.* **2010**, *22*, 3906–3924. [[CrossRef](#)]
30. Dikin, D.A.; Stankovich, S.; Zimney, E.J.; Piner, R.D.; Dommett, G.H.; Evmenenko, G.; Nguyen, S.T.; Ruoff, R.S. Preparation and characterization of graphene oxide paper. *Nature* **2007**, *448*, 457–460. [[CrossRef](#)]
31. Stankovich, S.; Dikin, D.A.; Piner, R.D.; Kohlhaas, K.A.; Kleinhammes, A.; Jia, Y.; Wu, Y.; Nguyen, S.T.; Ruoff, R.S. Synthesis of graphene-based nanosheets via chemical reduction of exfoliated graphite oxide. *Carbon* **2007**, *45*, 1558–1565. [[CrossRef](#)]
32. Deb, A.; Vimala, R. Camptothecin loaded graphene oxide nanoparticle functionalized with polyethylene glycol and folic acid for anticancer drug delivery. *J. Drug Deliv. Sci. Technol.* **2018**, *43*, 333–342. [[CrossRef](#)]
33. Li, D.; Gao, D.; Qi, J.; Chai, R.; Zhan, Y.; Xing, C. Conjugated Polymer/Graphene Oxide Complexes for Photothermal Activation of DNA Unzipping and Binding to Protein. *ACS Appl. Bio Mater.* **2018**, *1*, 146–152. [[CrossRef](#)]
34. Wei, W.; Qu, X. Extraordinary physical properties of functionalized graphene. *Small* **2012**, *8*, 2138–2151. [[CrossRef](#)] [[PubMed](#)]
35. Mao, H.Y.; Laurent, S.; Chen, W.; Akhavan, O.; Imani, M.; Ashkarran, A.A.; Mahmoudi, M. Graphene: Promises, facts, opportunities, and challenges in nanomedicine. *Chem. Rev.* **2013**, *113*, 3407–3424. [[CrossRef](#)] [[PubMed](#)]
36. Qi, J.; Lv, W.; Zhang, G.; Li, Y.; Zhang, G.; Zhang, F.; Fan, X. A graphene-based smart catalytic system with superior catalytic performances and temperature responsive catalytic behaviors. *Nanoscale* **2013**, *5*, 6275–6279. [[CrossRef](#)]
37. Navalon, S.; Dhakshinamoorthy, A.; Alvaro, M.; Antonietti, M.; Garcia, H. Active sites on graphene-based materials as metal-free catalysts. *Chem. Soc. Rev.* **2017**, *46*, 4501–4529. [[CrossRef](#)]

38. Gerber, I.C.; Serp, P. A Theory/Experience Description of Support Effects in Carbon-Supported Catalysts. *Chem. Rev.* **2020**, *120*, 1250–1349. [[CrossRef](#)]
39. Yan, P.; Zhang, B.; Wu, K.-H.; Su, D.; Qi, W. Surface chemistry of nanocarbon: Characterization strategies from the viewpoint of catalysis and energy conversion. *Carbon* **2019**, *143*, 915–936. [[CrossRef](#)]
40. Martí, M.; Frigols, B.; Salesa, B.; Serrano-Aroca, Á. Calcium alginate/graphene oxide films: Reinforced composites able to prevent *Staphylococcus aureus* and methicillin-resistant *Staphylococcus epidermidis* infections with no cytotoxicity for human keratinocyte HaCaT cells. *Eur. Polym. J.* **2019**, *110*, 14–21. [[CrossRef](#)]
41. Salesa, B.; Martí, M.; Frigols, B.; Serrano-Aroca, A. Carbon Nanofibers in Pure Form and in Calcium Alginate Composites Films: New Cost-Effective Antibacterial Biomaterials against the Life-Threatening Multidrug-Resistant *Staphylococcus epidermidis*. *Polymers (Basel)* **2019**, *11*, 453. [[CrossRef](#)] [[PubMed](#)]
42. Akhavan, O.; Ghaderi, E.; Esfandiari, A. Wrapping bacteria by graphene nanosheets for isolation from environment, reactivation by sonication, and inactivation by near-infrared irradiation. *J. Phys. Chem. B* **2011**, *115*, 6279–6288. [[CrossRef](#)]
43. Tan, S.; Wu, X.; Xing, Y.; Lilak, S.; Wu, M.; Zhao, J.X. Enhanced synergetic antibacterial activity by a reduce graphene oxide/Ag nanocomposite through the photothermal effect. *Colloids Surf. B Biointerfaces* **2020**, *185*, 110616. [[CrossRef](#)] [[PubMed](#)]
44. Hui, L.; Auletta, J.T.; Huang, Z.; Chen, X.; Xia, F.; Yang, S.; Liu, H.; Yang, L. Surface Disinfection Enabled by a Layer-by-Layer Thin Film of Polyelectrolyte-Stabilized Reduced Graphene Oxide upon Solar Near-Infrared Irradiation. *ACS Appl. Mater. Interfaces* **2015**, *7*, 10511–10517. [[CrossRef](#)] [[PubMed](#)]
45. Gao, S.; Zhang, L.; Wang, G.; Yang, K.; Chen, M.; Tian, R.; Ma, Q.; Zhu, L. Hybrid graphene/Au activatable theranostic agent for multimodalities imaging guided enhanced photothermal therapy. *Biomaterials* **2016**, *79*, 36–45. [[CrossRef](#)] [[PubMed](#)]
46. Chen, Y.W.; Su, Y.L.; Hu, S.H.; Chen, S.Y. Functionalized graphene nanocomposites for enhancing photothermal therapy in tumor treatment. *Adv. Drug Deliv. Rev.* **2016**, *105*, 190–204. [[CrossRef](#)]
47. Wang, Y.; Wang, H.; Liu, D.; Song, S.; Wang, X.; Zhang, H. Graphene oxide covalently grafted upconversion nanoparticles for combined NIR mediated imaging and photothermal/photodynamic cancer therapy. *Biomaterials* **2013**, *34*, 7715–7724. [[CrossRef](#)]
48. Wang, Y.; Li, Z.; Wang, J.; Li, J.; Lin, Y. Graphene and graphene oxide: Biofunctionalization and applications in biotechnology. *Trends Biotechnol.* **2011**, *29*, 205–212. [[CrossRef](#)]
49. Horváth, L.; Magrez, A.; Burghard, M.; Kern, K.; Forró, L.; Schwaller, B. Evaluation of the toxicity of graphene derivatives on cells of the lung luminal surface. *Carbon* **2013**, *64*, 45–60. [[CrossRef](#)]
50. Zhen, X.; Xie, C.; Jiang, Y.; Ai, X.; Xing, B.; Pu, K. Semiconducting Photothermal Nanoagent for Remote-Controlled Specific Cancer Therapy. *Nano Lett.* **2018**, *18*, 1498–1505. [[CrossRef](#)]
51. Huang, Y.; Lai, Y.; Shi, S.; Hao, S.; Wei, J.; Chen, X. Copper sulfide nanoparticles with phospholipid-PEG coating for in vivo near-infrared photothermal cancer therapy. *Chem. Asian J.* **2015**, *10*, 370–376. [[CrossRef](#)] [[PubMed](#)]
52. Li, J.; Duan, H.; Pu, K. Nanotransducers for Near-Infrared Photoregulation in Biomedicine. *Adv. Mater.* **2019**, *31*, e1901607. [[CrossRef](#)] [[PubMed](#)]
53. Zhu, C.; Yang, Q.; Liu, L.; Wang, S. A potent fluorescent probe for the detection of cell apoptosis. *Chem Commun (Camb)* **2011**, *47*, 5524–5526. [[CrossRef](#)] [[PubMed](#)]
54. Wang, Y.-W.; Fu, Y.-Y.; Wu, L.-J.; Li, J.; Yang, H.-H.; Chen, G.-N. Targeted photothermal ablation of pathogenic bacterium, *Staphylococcus aureus*, with nanoscale reduced graphene oxide. *J. Mater. Chem. B* **2013**, *1*, 2496. [[CrossRef](#)]
55. Jia, X.; Ahmad, I.; Yang, R.; Wang, C. Versatile graphene-based photothermal nanocomposites for effectively capturing and killing bacteria, and for destroying bacterial biofilms. *J. Mater. Chem. B* **2017**, *5*, 2459–2467. [[CrossRef](#)]
56. Sanchez, V.C.; Jachak, A.; Hurt, R.H.; Kane, A.B. Biological interactions of graphene-family nanomaterials: An interdisciplinary review. *Chem. Res. Toxicol.* **2012**, *25*, 15–34. [[CrossRef](#)]
57. Wu, M.; Kempaiah, R.; Huang, P.J.; Maheshwari, V.; Liu, J. Adsorption and desorption of DNA on graphene oxide studied by fluorescently labeled oligonucleotides. *Langmuir* **2011**, *27*, 2731–2738. [[CrossRef](#)]
58. Akhavan, O.; Ghaderi, E. Toxicity of Graphene and Graphene Oxide Nanowalls Against Bacteria. *ACS Nano* **2010**, *4*, 5731–5736. [[CrossRef](#)]

59. Nel, A.; Xia, T.; Mädler, L.; Li, N. Toxic Potential of Materials at the Nanolevel. *Science* **2006**, *311*, 622–627. [[CrossRef](#)]
60. Perreault, F.; de Faria, A.F.; Nejati, S.; Elimelech, M. Antimicrobial Properties of Graphene Oxide Nanosheets: Why Size Matters. *Acs Nano* **2015**, *9*, 7226–7236. [[CrossRef](#)]
61. Tu, Y.; Lv, M.; Xiu, P.; Huynh, T.; Zhang, M.; Castelli, M.; Liu, Z.; Huang, Q.; Fan, C.; Fang, H.; et al. Destructive extraction of phospholipids from Escherichia coli membranes by graphene nanosheets. *Nat. Nanotechnol.* **2013**, *8*, 594–601. [[CrossRef](#)] [[PubMed](#)]



© 2020 by the authors. Licensee MDPI, Basel, Switzerland. This article is an open access article distributed under the terms and conditions of the Creative Commons Attribution (CC BY) license (<http://creativecommons.org/licenses/by/4.0/>).